Electronic Supplementary Material (ESI) for Nanoscale Advances.

Supplementary Information for

Impact of organic phosphates on the structure and composition of short-range ordered iron phases

Zhengzheng Chen,[a,b,*] Jeffrey Paulo H. Perez,[a,*] Glen J. Smales,[c] Roberts Blukis,[a,†] Brian R. Pauw,[c] Jessica A. Stammeier,[a] Jörg Radnik,[c] Andrew Smith,[d] Liane G. Benning [a,b]

[a] *GFZ German Research Center for Geosciences, Telegrafenberg, 14473 Potsdam, Germany*

[b] *Department of Earth Sciences, Freie Universität Berlin, Malteserstraße 74-100, 12249 Berlin, Germany*

[c] *Bundesanstalt für Materialforschung und-prüfung (BAM), Unter den Eichen 87, 12205 Berlin, Germany*

[d] *Diamond Light Source, Harwell Science and Innovation Campus, Didcot, Oxfordshire, OX11 0DE, United Kingdom*

[†] *Current affiliation: Leibniz-Institut für Kristallzüchtung (IKZ), Berlin 12489, Germany*

Corresponding authors: zhchen@gfz-potsdam.de, jpperez@gfz-potsdam.de

This supporting information contains: 23 pages, 10 figures and 8 tables.

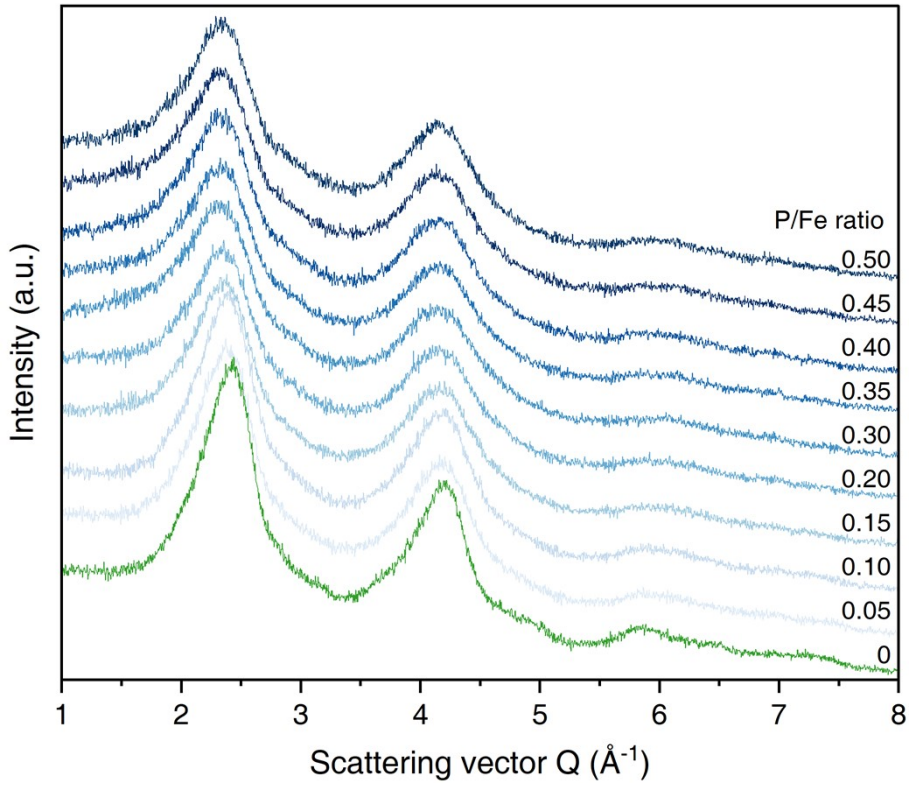

Figure S1. XRD patterns of GP-free and GP-FHY coprecipitates. Series labels represent different nominal molar P/Fe ratios.

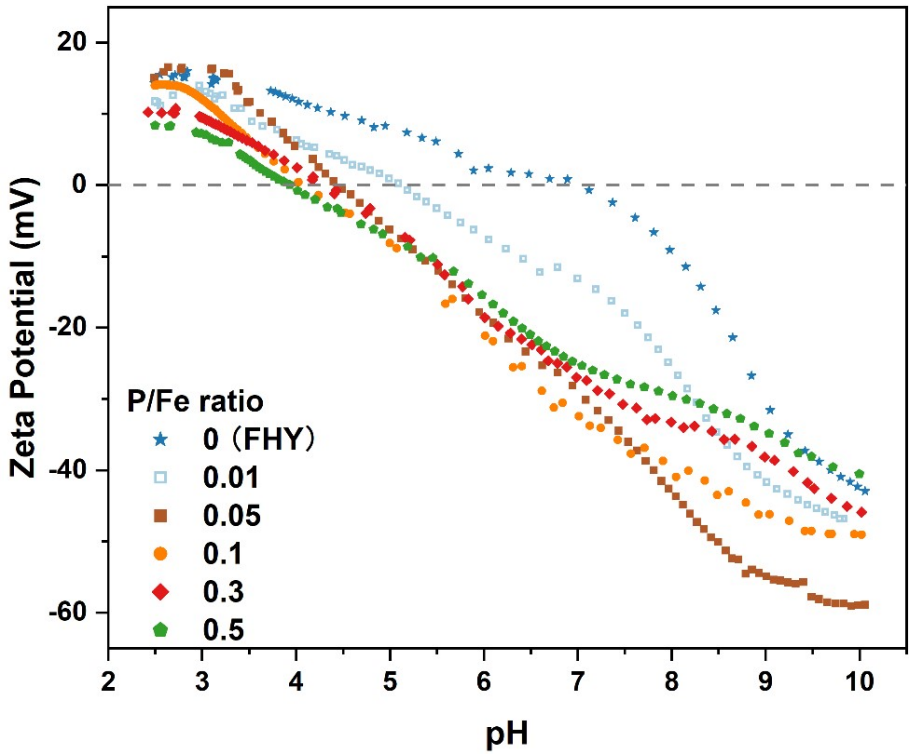

Figure S2. Zeta potentials of GP-free and GP-FHY coprecipitates as a function of pH. Zeta potentials were determined in 10 mM NaCl at solid concentrations of 0.4 g L^{-1}.

Table S1. ICP-OES data for quality control (QC).

	Fe (µg/g)	P (µg/g)	Na (µg/g)
Wavelength (nm)	261.382	213.618	589.592
Matrix	**0.3 M HNO_3 + 1000 ppm Cs**		
Instrumental limits			
Limit of detection (LoD)	0.018	0.006	0.018
Limit of quantification (LoQ)	0.029	0.018	0.032
Quality control			
QC verify (*n*= 8)	0.427	0.208	0.441
SD	0.007	0.003	0.007
RSD	2%	1%	2%
2RSD	3%	3%	3%
Reference value	0.408	0.204	0.423
Uncertainty of reference value	0.001	0.010	0.001
Measured deviation from reference value	4%	2%	4%
Matrix	**0.3 M HNO_3 + 0.075 M HCl + 1000 ppm Cs**		
Instrumental limits			
Limit of detection (LoD)	0.021	0.004	
Limit of quantification (LoQ)	0.037	0.009	
Quality control			
QC verify (*n* = 3)	0.413	0.206	
SD	0.005	0.004	
RSD	1%	2%	
2RSD	2%	3%	
Reference value	0.408	0.200	
Uncertainty of reference value	0.001	0.001	
Measured deviation from reference value	1%	3%	

Elemental concentration of suspension and coprecipitates measured by ICP-OES[1]

All filtered supernatants for ICP-OES analyses were acidified with concentrated HNO_3 (Merck, Suprapure grade) to a final HNO_3 concentration of 0.3 M and stored in acid-cleaned polypropylene (PP) tubes at 4°C. For the FHY and coprecipitate suspensions, 100 µL was collected into a PP tube containing 10 mL of 0.3 M HNO_3. The pH of 0.3 M HNO_3 was < 2, which was sufficient to completely dissolve the newly formed iron(III) hydroxide phases. In

addition, ~20 mg of freeze-dried coprecipitates were digested with 1 M HCl and diluted by Milli-Q water to a Fe concentration of ~120 mg L^{-1} and stored in acid-cleaned PP bottles at 4°C.

Acidified liquid samples were diluted gravimetrically with 0.3 M HNO_3 containing cesium (Cs, 1 mg g^{-1}) and scandium (Sc, 1 µg g^{-1}), as an ionization buffer and internal standard, respectively. The calibration standards were prepared by mixing single ICP elements standards (Merck Certipur, traceable to NIST reference materials) in the same matrix as the diluted samples, except that standards for HCl-digested coprecipitates additionally contained 0.075 M HCl. Dilution factors ranging from 1.33 to 150 were used to ensure that the analyte solutions were within the concentration range of the matrix-matched calibration standards (linearity criteria R^2 >0.9990).

For each analytical session, instrument stability and drift were monitored for each sample analysis using Ar, Cs and Sc at emission wavelengths of 420.067, 459.311 and 335.372 nm, respectively, and quality control (QC) solutions with similar sample composition were measured at regular intervals. Instrument statistical limits of detection (LoD = 3SD above background) or limits of quantification (LoQ = 10SD above background) were determined in each analytical session based on eight repeat analyses of 0.3 M HNO_3 (+ 1 mg g^{-1} Cs) and three repeat analyses of 0.3 M HNO_3 + 0.075 M HCl (+ 1 mg g^{-1} Cs) used for sample dilution. Concentrations of Fe, P and Na in the samples were evaluated using the emission wavelengths of 261.382, 213.618 and 589.592 nm, respectively. Analytical uncertainties at a 95% confidence level for concentrations quantified (above LoQ) during this study are ~5% relative, verified by repeat analyses of a QC solution, which was similar to the sample compositions (Table S1).

Adsorption batch experiments

To determine the maximum adsorption capacity of FHY, batch experiments were conducted by adding an amount of FHY slurry to a GP solution, both at an initial pH of 7. The final 10 mL system had an Fe(III) concentration of 5 mM and a GP concentration of 0.01 – 10 mM (nominal P/Fe molar ratios = 0.002 – 2) and were shaken at 150 rpm for 24 h in an orbital shaker. The suspensions were centrifuged at 7690×*g* for 5 min and the liquid phases were filtered through a 0.22-µm polyvinylidene difluoride (PVDF) syringe filter. The filtered solutions were acidified with concentrated HNO_3 (Aristar® for trace element analysis), stored at 4 °C to determine GP concentration by ICP-OES. Each batch included triplicate samples (B1, B2 and B3) with three blanks (GP only) and one control (FHY only) for each GP concentration. Only precipitates with initial GP concentration of 0.5, 1.0, and 2.0 mM (nominal P/Fe molar ratios = 0.1, 0.2 and 0.4) were freeze-dried for surface area and porosity measurement.

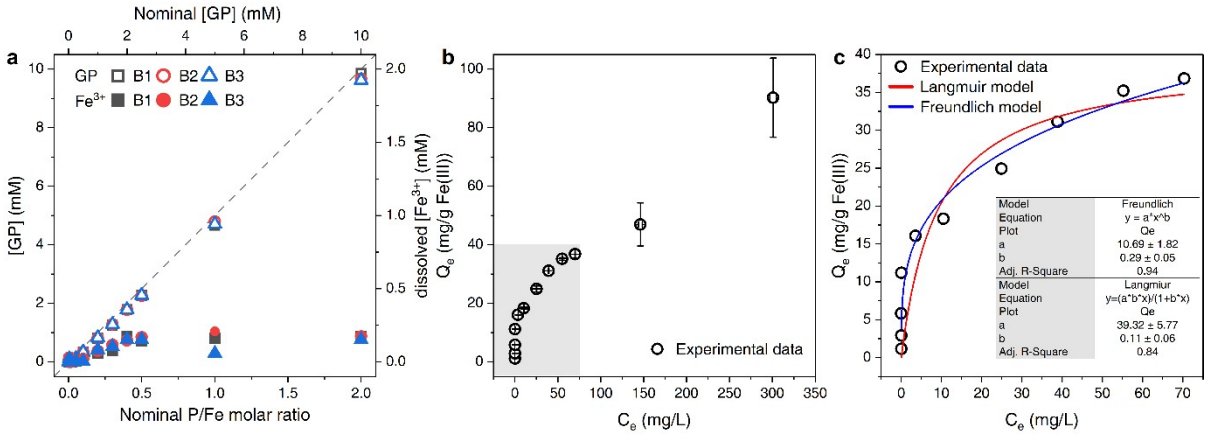

Figure S3. [GP](empty symbols) and [Fe^{3+}] (solid symbols) in the supernatant of the adsorption experiment in triplicate (B1, B2 and B3). Grey dashed line for sight guidance. Adsorption of GP on FHY(b), and as FHY dissolves in higher concentrations of GP (P/Fe = 1,2), the Langmuir and Freundlich models were used to fit the data in the grey marked range(c). According to the Langmuir fitting result, the maximum adsorption capacity of P in GP was 39.3 mg g^{-1} Fe(III), indicating that the maximum molar $P/Fe_{(s)}$ ratio reachable via adsorption is 0.07.

Surface composition of solid precipitates measured by X-ray photoelectron spectroscopy

All measurements were performed with an AXIS Ultra DLD photoelectron spectrometer manufactured by Kratos Analytical (Manchester, UK). XPS spectra were recorded using monochromatized aluminum Kα radiation for excitation, at a pressure of approximately 5 × 10^{-9} mbar. The electron emission angle was 0° and the source-to-analyzer angle was 60°. The binding energy scale of the instrument was calibrated following a Kratos Analytical procedure which uses ISO 15472 binding energy data. Spectra were taken by setting the instrument to the hybrid lens mode and the slot mode providing approximately a 300 × 700 μm^2 analysis area. Furthermore, the charge neutralizer was used. Survey spectra were recorded with a step size of 1 eV and a pass energy of 80 eV, high-resolution spectra were recorded with a step size of 0.1 eV and a pass energy of 20 eV. Quantification was performed with Unifit 2021 using Scofield factor, the inelastic mean free pathway and the transmission function for the normalization of the peak area. For peak fitting, a sum Gaussian-Lorentzian function was used. A modified Tougaard background was used to determine the background.

Table S2. Deconvolution and interpretation of high-resolution O 1s XPS spectra.

P/Fe ratio	Peak assignment	Binding energy (eV) [a]	FWHM (eV) [b]	Relative area (%) [c]	Surface composition (%)
0.05	O oxide	529.9	1.27	52.2 ± 10.4	52.2 ± 10.4
	Organic O, OH	531.1	1.27	30.0 ± 6.0	43.6 ± 6.6
	Organic O	532.1	1.27	13.6 ± 2.7	
	$(PO_3)^-$	533.3	1.27	4.2 ± 0.8	4.2 ± 0.8
0.5	O oxide	529.2	1.38	23.1 ± 4.6	23.1 ± 4.6
	Organic O, OH	530.4	1.38	39.4 ± 7.9	66.2 ± 9.3
	Organic O	531.7	1.38	23.8 ± 4.8	
		533.8	1.38	2.9 ± 0.6	
	$(PO_3)^-$	532.7	1.38	10.7 ± 2.1	10.7 ± 2.1

Note: [a] Uncertainty of the binding energy is ± 0.2 eV with a confidence interval of 95 %; [b] full width at half-maximum; [c] relative uncertainty of quantification is ± 20% with a confidence interval of 95 %.

Surface area and porosity of solid precipitates

Freeze-dried samples were degassed at 120 °C under vacuum for 4 h and the final mass of dried sample in the cell was approximately 100-200 mg. N_2 adsorption/desorption isotherms and porosity were measured at 77 K over the relative pressure range (P/P_0) from 0.01 to 0.999 (Micromeritics Gemini VII 2390 Surface Area Analyzer). The Brunauer–Emmett–Teller (BET) surface areas (SSA) were calculated on the linear part of the Rouquerol plot in the range of 0.01-0.20 P/P_0.[2,3] The pore size distribution was determined by the Barrett-Joyner-Halenda (BJH) model using desorption isotherms, and the total pore volumes (V) were calculated from sorption isotherms at P/P_0 = 0.95.[4] The surface area and total pore volume have been corrected by considering the effect of glycerol phosphate content using the following equations:

$$SSA_{corr} = \frac{SSA}{1 - \frac{[GP]}{1000}} \qquad (Eq.\,S1)$$

$$V_{corr} = \frac{V}{1 - \frac{[GP]}{1000}} \qquad (Eq.\,S2)$$

where SSA ($m^2\ g^{-1}$) and V ($cm^3\ g^{-1}$) were calculated from N_2 adsorption/desorption isotherms and GP refers to glycerol phosphate concentration ($mg\ g^{-1}$).[5]

Table S3. Surface area and total pore volume of FHY and FGY-GP coprecipitates.

Nominal P/Fe ratio	SSA_{corr} ($m^2\ g^{-1}$)		V_{corr} ($cm^3\ g^{-1}$)	
	Batch 1	Batch 2	Batch 1	Batch 2
0	296	283	0.171	0.173
0.01	316	327	0.165	0.180
0.05	270	274	0.131	0.138
0.10	195	187	0.129	0.131
0.15	191	191	0.076	0.075
0.20	121	121	0.048	0.047
0.30	121	68	0.044	0.025
0.35	144	4	0.051	0.002
0.40	40	131	0.016	0.049
0.45	149	5	0.058	0.003
0.50	4	1	0.002	0.002

Table S4. The properties of coprecipitates of FHY and different phosphorus compounds.

P compounds	P/Fe	$P/Fe_{(s)}$	surface area ($m^2\ g^{-1}$)	zeta potential* (mV)	Refs.
inorganic phosphate	0.05	0.05	333	23	Santoro et al.[6]
	0.10	0.11	317	12	
	0.50	0.47	194	2	
inositol hexaphosphate	0.05	0.05	279	20	
	0.10	0.11	264	8	
	0.50	0.48	193	-38	
phosphatidylcholine	0.05	0.05	~31	34	
	0.10	0.11	~2	22	
	0.50	0.44	~5	7	
GP	0.05	0.05	272	-16	This work
	0.10	0.10	191	-22	
	0.50	0.22	3	-14	

Note: * In the study by Santoro et al. the zeta potential of freshly synthesized samples was measured at pH 6.

Small-angle X-ray scattering (SAXS) measurements

Data from the MOUSE instrument at BAM was collected using an in-vacuum Eiger 1M detector (Dectris, Switzerland) with X-rays generated from microfocus X-ray tubes, followed by multilayer optics to parallelize and monochromatize the X-ray beams to wavelengths of Cu Kα (λ = 0.154 nm) and Mo Kα (λ = 0.711 nm). Data from I22 was collected using a Pilatus3 2M detector (Dectris, Switzerland) with X-rays of an energy of 18 keV (λ = 0.0689 nm). The sample to detector distance was 9.7425 m, calibrated using a 100 nm period Si3N4 grating (Silson, UK). Both data sets were combined to ensure a broad overlap between the different measurement ranges. Data from the different instruments were consistent as they are processed using the collaboratively developed comprehensive universal data correction pipeline.[7] The data was then merged, weighted by the data point uncertainty, in the overlapping regions using the DataMerge method, the most current version of which can be found here.[8] SAXS data analysis was performed using the SASfit software package.[9] The scattering pattern is modelled (Figure S5). For this model, the smallest sphere contribution represents the primary beads (oligomers/clusters). As this is present in the sample as a well-ordered structure a hard-sphere structure factor has been added to this component. The largest-sized sphere contribution, at the smallest q, represents the sample particles. To account for the polydispersity inherent in these sphere populations, all three populations are compounded with a log-normal size distribution.

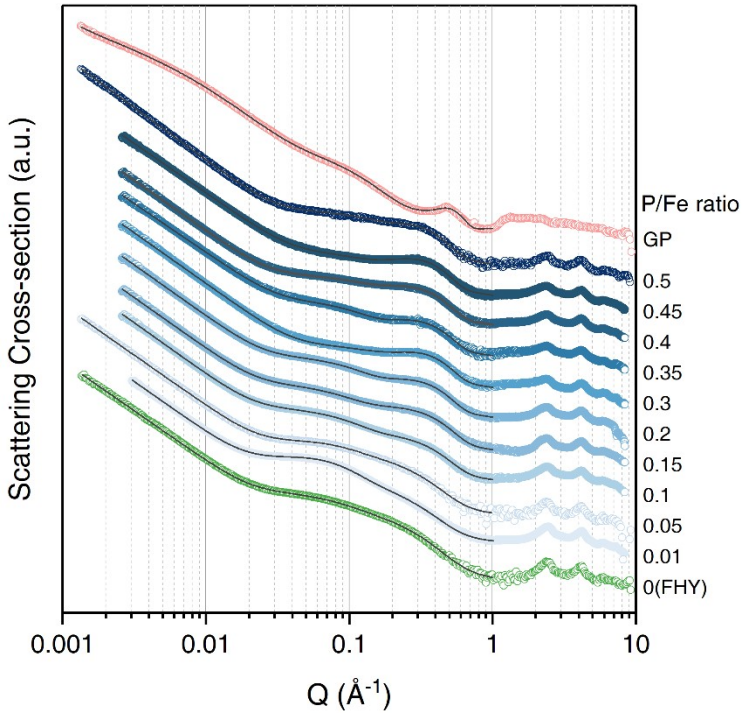

Figure S4. SAXS curves for GP, and GP-free and GP-FHY coprecipitates synthesized at different P/Fe ratios.

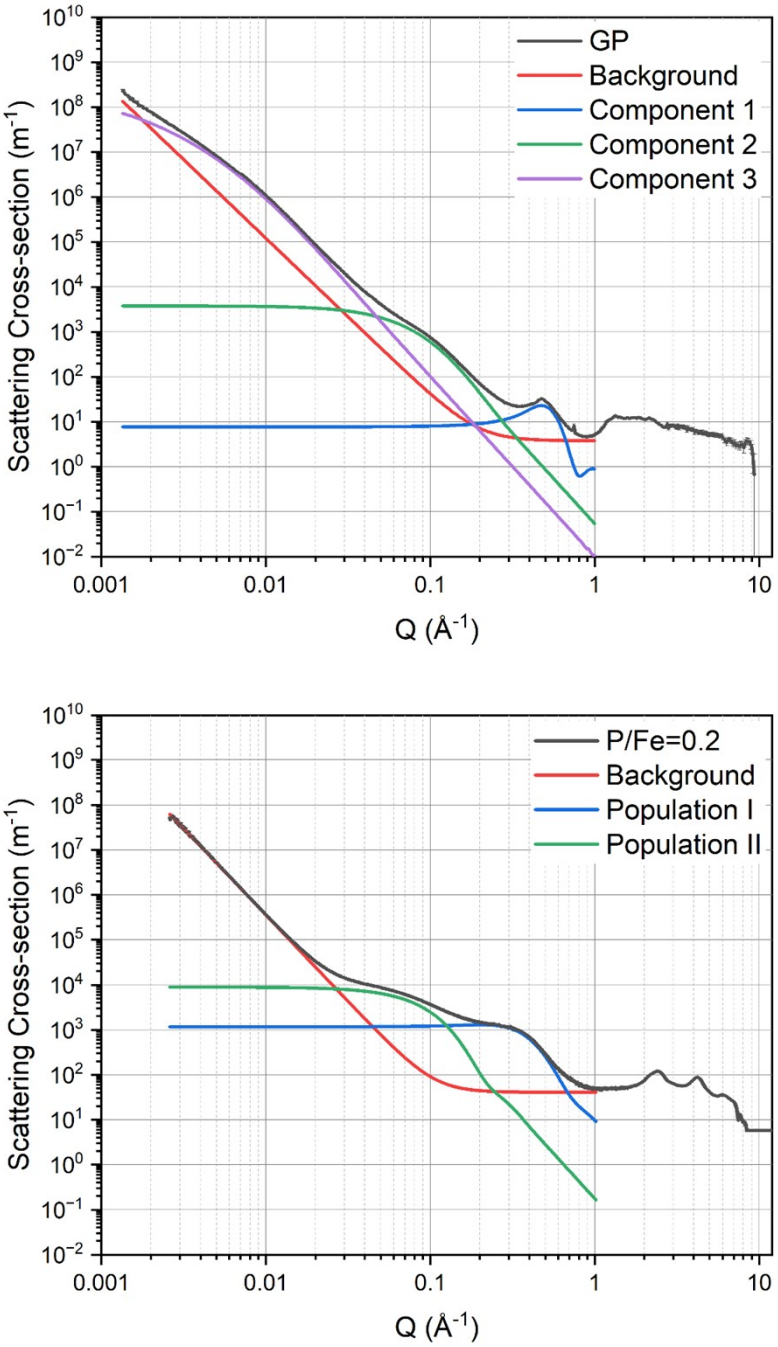

Figure S5. SAXS curves with spherical models for GP (top) and the coprecipitate at P/Fe ratio of 0.2 (bottom) as examples.

Fourier-transform infrared spectroscopy (FTIR)

In order to achieve a better peak assignment, the IR spectra of (de)protonated GP were obtained by adjusting the pH of the GP solutions, since the protonated GP may share similarities with the iron-complexed GP in terms of peak intensity, shift and (dis)appearance. In Figure S8, GP (pK_{a1}=1.33 and pK_{a2}=6.65) is largely in the form of zero-valent (H_2L), monovalent (HL^-) and divalent (L^{2-}) anions in solutions at pH values of 1, 4-6 and 7-9, respectively. Previous studies have shown that the broad peak appearing at ~1200 is likely to be associated with hydrogen bonded atoms and thus assigned to the δ(PO···H), while peak at ~1120 cm^{-1} becomes weaker at lower pH and is therefore designated as ν(P=O).[10,11] The IR spectral features of GP are strongly pH-dependent, as shown by the decreasing peaks at 1100 and 1080 cm^{-1} with increasing pH and are therefore attributed to ν_s(P-O_2) and ν_s(P-O) vibrations respectively.[12] In contrast, the relative intensities of the peaks at 1060 and 1000 cm^{-1} are positively correlated with the protonation of GP, becoming apparent and boarder at pH 6 and 1, respectively, and thus assigned to the asymmetric vibrations of P-OH and P-$(OH)_2$. The peak at 1040 cm^{-1} was observed at all studied pH values, which is consistent with Li et al.[13] attributing this peak to the asymmetric stretching of P-O-C. However, at any pH value, no peaks were found in the 1030-1050 cm^{-1} frequency range in the IR spectra of phosphate,[11] but can be detected for iron-complexed with phosphate,[11,14,15] and some organic phosphates such as GP,[13] phosphate diesters,[16] glucose-1-phosphate,[17] monomethyl phosphate[18] and phytates,[19] we therefore suggest that this may be an asymmetric vibration of the P-OX (*X* = metal or C). Furthermore, similar peaks of 970 cm^{-1} became broader at lower pH values and can therefore be assigned to ν(P-OH) or ν_s(P-O*X*).[10] Lastly, peaks at ~910 and ~940 cm^{-1} are clearly associated with P-OH vibration, while peak at 960 cm^{-1} is probably attributed to the P-O stretching in completely deprotonated phosphate group.[13] Peak assignment of GP at pH 9, 6 and 1 can be found in Table S5.

Table S5. FTIR frequencies (in cm^{-1}) and group assignment of GP at pH of 9, 6, and 1 and coprecipitates at P/Fe ratios of 0.05, 0.3 and 0.5

Glycerol phosphate				GP-FHY				Bonding geometry	Refs.
pH 9 L^{2-}	pH 6 HL^-	pH 1 H_2L	Assignment	0.05	0.3	0.5	Assignment		
	910	915	-		885	891	ν_s(P–OH)	^1V	11,20
959	929	940	-						
975	973	971	ν(P-OH)	970	965	968	ν_s(P–O–Fe)	^1V	10,16,21
994	999	1006	ν_{as}(P–$(OH)_2$)	999	998	1003	ν_{as}(P–$(O–Fe)_2$)	^2C	10,22
1044	1043	1040	ν_{as}(P–O–C)	1045	1043	1043	ν_{as}(P–O–Fe)	^2C	*See Text above*
	1060	1057	ν_{as}(P–O–H)						
1081	1082	1085	ν_s(P-O)	1080	1075	1077	ν_s(P–O)	^1V	12
1106	1102		$\nu_s(PO_2)$						
1124	1119	1114	ν(P=O)	1125	1115	1115	ν(P=O)	^2C to ^1V	11,12
					1149	1150	$\nu_s(PO_2)$	^1V	12
	1185	1186	δ(P–O–H)						21

ν = stretching; δ = bending; as = asymmetric, s = symmetric

Table S6. Peak position and relative area for curve fitting of IR spectra in the phosphate region

P/Fe ratio		Batch 1							Batch 2						
0.05			970	999	1045	1080	1125			970	1000	1045	1080	1126	
0.1		899	966	998	1045	1075	1112	1145	900	967	999	1045	1075	1112	1144
0.15		887	965	997	1044	1074	1112	1144	886	965	997	1044	1073	1112	1144
0.2	Centre	886	964	997	1043	1074	1110	1143	886	964	997	1043	1074	1111	1144
0.3	position	885	965	998	1043	1075	1115	1149	886	965	998	1043	1074	1116	1150
0.35	(cm^{-1})	888	965	998	1042	1071	1115	1149	893	964	1001	1042	1071	1112	1149
0.4		890	965	1001	1042	1071	1113	1150	889	965	1001	1042	1071	1114	1149
0.45		891	965	1001	1042	1071	1113	1151	894	964	999	1043	1071	1113	1150
0.5		895	969	1003	1043	1077	1115	1150	894	970	1004	1043	1076	1115	1150
0.05			22	12	22	22	21			21	12	23	23	21	
0.1		5	26	15	20	13	15	6	4	26	15	20	13	16	5
0.15		4	29	14	17	14	14	7	4	29	14	17	14	15	7
0.2	Relative	5	28	15	18	13	14	8	4	29	15	18	13	14	8
0.3	area	4	32	13	16	15	16	4	4	32	13	16	15	16	4
0.35	(%)	4	32	13	15	16	17	4	5	29	15	16	14	16	4
0.4		6	29	15	16	15	15	4	7	29	15	15	15	16	4
0.45		6	29	15	15	15	16	4	5	30	16	15	14	18	3
0.5		6	31	10	20	15	13	5	6	32	10	15	17	18	3

Note: the intensity of the coprecipitates with the P/Fe ratio of 0.01 is too low (see Figure S6) to give a good curve fit and is therefore not given here. Values on the light blue background are assigned to ^{2}C geometry, others represent ^{1}V geometry

Table S7. FTIR frequencies (in cm^{-1}) and group assignment of FHY and coprecipitates for full range.

Wavenumbers (cm^{-1})	Assignments	Comment
~3360	ν(OH)[323,24]	Surface hydroxyl groups
~3220	ν(OH)[31]	Bulk hydroxyl groups
~2960	$\nu_{as}(CH_2)$[25]	Organic moiety of GP
~2875	$\nu_{s}(CH_2)$[25]	Organic moiety of GP
~1645-1630	δ_{s} (HOH)[23,24]	Bending of adsorbed water
~1470	$\delta_{as}(CH_2)$ /δ_{as} (CH_3)[25]	Organic moiety of GP
~1395	ν_{s}(C–O)[25]	Organic moiety of GP
~1350	δ(OH)[23]	OH bending
~1150	$\nu_{s}(PO_2)$	PO_4 group complexed with Fe
~1125-1115	ν(P=O)	(See Table S5 for references)
~1080-1075	ν_{s}(P–O)	
~1045	ν_{as}(P–O–Fe)	
~1000	$\nu_{as}(P–(O–Fe)_2)$	
~970	ν_{s}(P–O–Fe)	
~890	ν_{s}(P–OH)	
~700-710	ν(Fe-O)	Fe-O stretching [23,24]
~590	ν(Fe-O)	
~442	ν(Fe-O)	

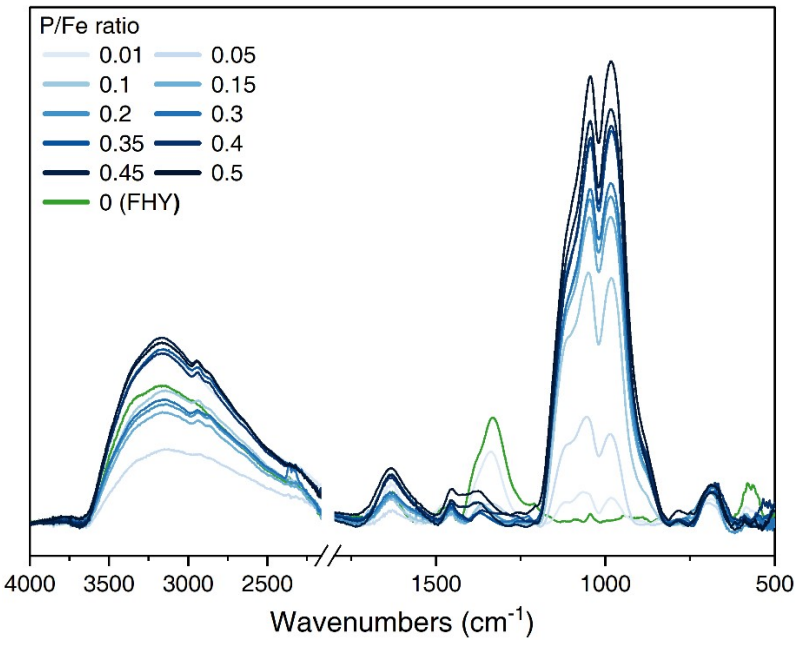

Figure S6. Full FTIR spectra of GP-free and GP-FHY coprecipitates synthesized at different nominal P/Fe molar ratios.

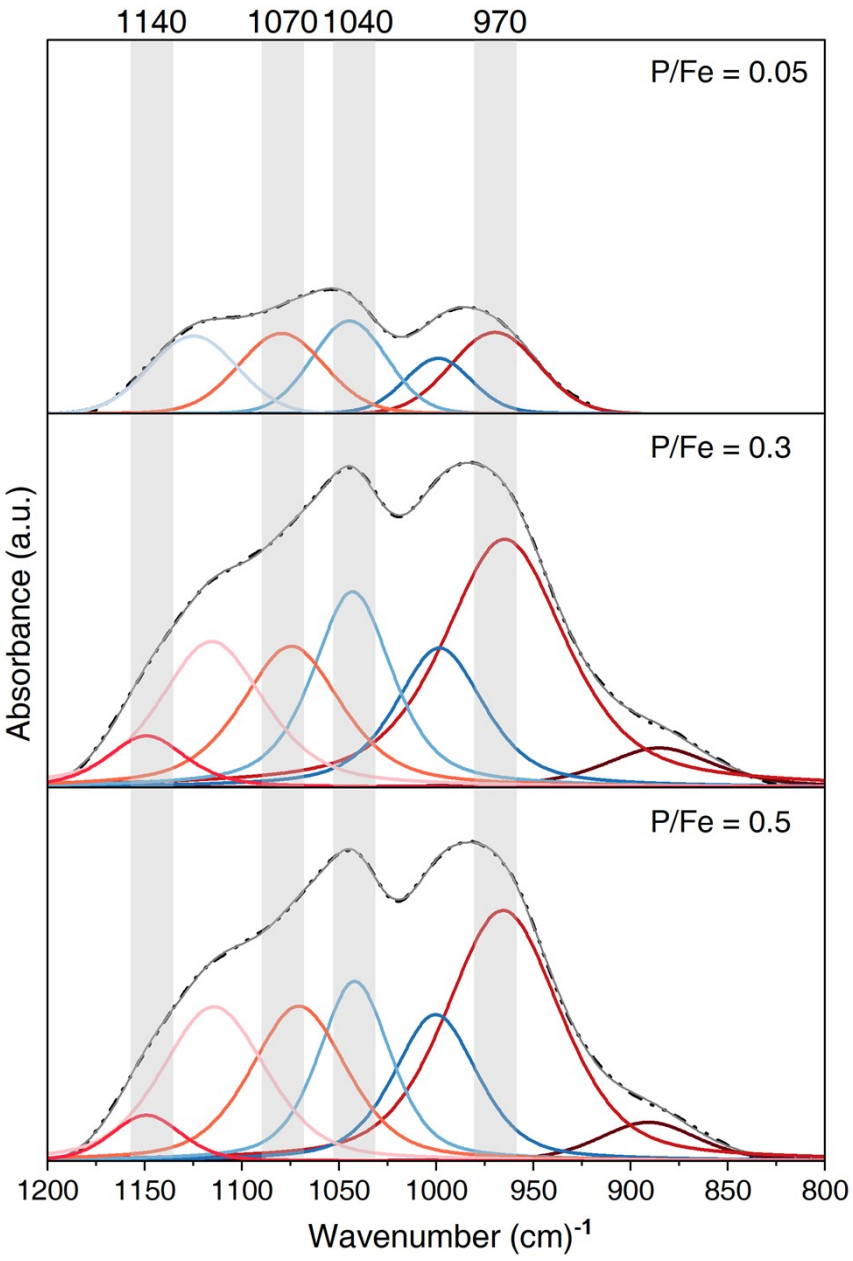

Figure S7. Deconvolution of the component bands of phosphate region (1200 – 800 cm^{-1}) the FTIR spectra for GP-FHY coprecipitations. Black dashed dotted lines denote the fitted spectra (component sum) and gray solid lines indicate experimental data. For the component bands, red lines indicate bands assigned with ^{1}V geometry and blue lines denote ^{2}C geometry.

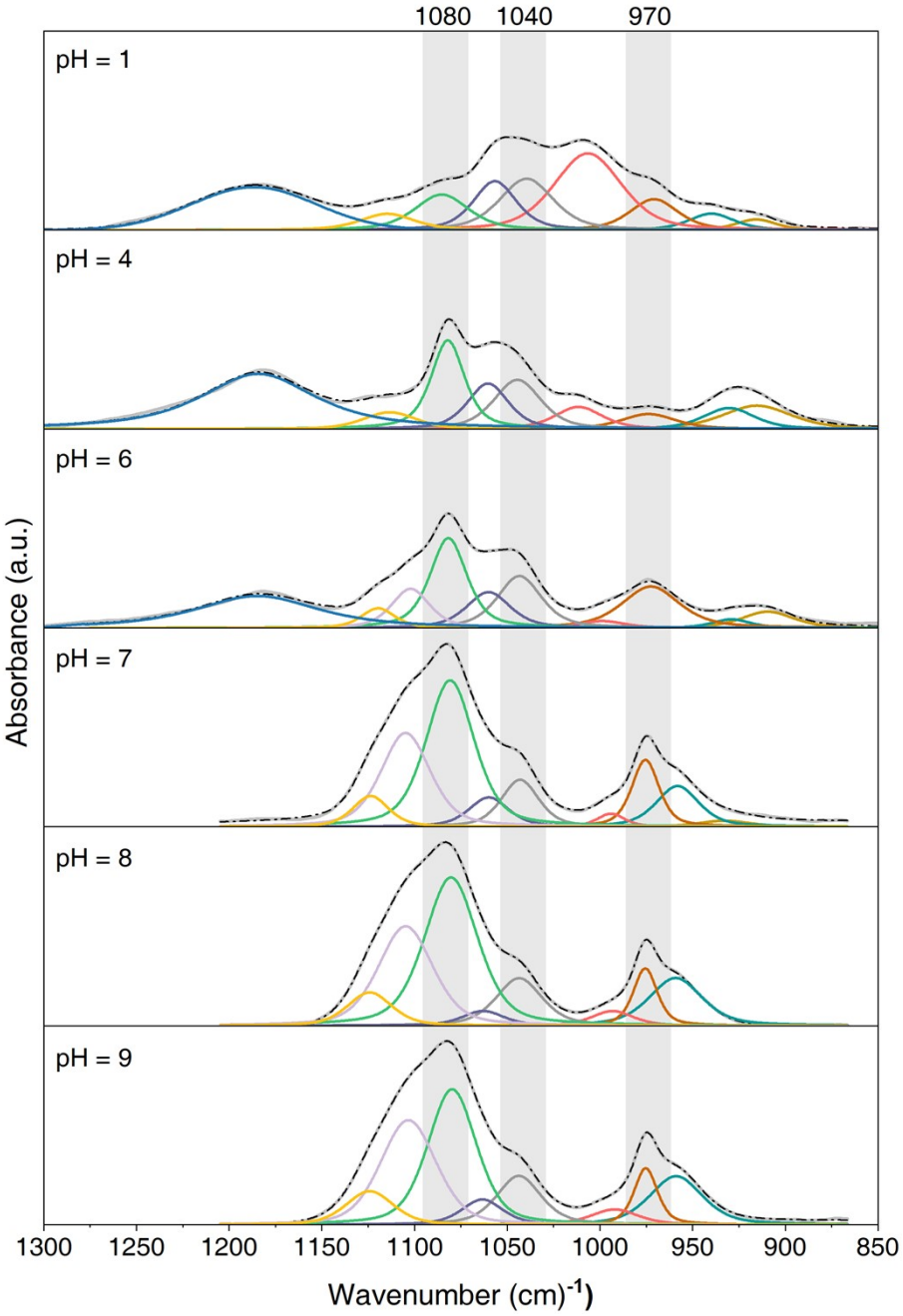

Figure S8. FTIR spectra of aqueous GP concentrations at different pH. Black dashed lines denote the fitted spectra (component sum) and gray solid lines indicate experimental data. Component bands assigned to P-O(*X*) stretching vibrations are marked in gray rectangles.

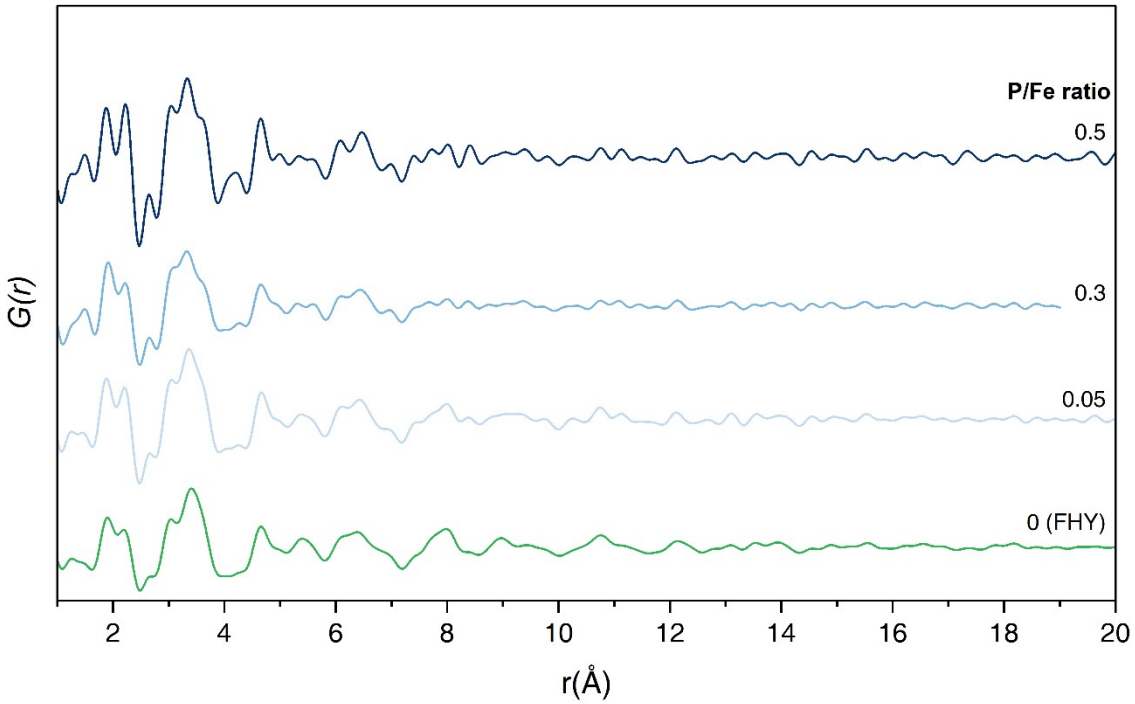

Figure S9. PDFs [*G(r)*] of GP-free and GP-FHY coprecipitates with nominal P/Fe molar ratios of 0.05, 0.3 and 0.5.

Iron K-edge extended X-ray absorption fine structure (EXAFS)

Sample preparation

Prior to data collection, 5 mg of freeze-dried powder samples were mixed with 65 mg cellulose to prepare pellets based on the calculation from XAFSmass software.[26] The pellets were sealed between 2-layers of 70-μm thick Kapton® polyimide tape and fixed onto custom sample holders. Iron K-edge XAS data were collected at BM23 of the European Synchrotron Radiation Facility (ESRF, Grenoble, France).

Measurement details and data processing

Samples were measured in a liquid nitrogen cryostat (77 K) with helium convection. Spectra were recorded in transmission mode out to a reciprocal space value of 14 Å^{-1}. The size of X-ray beam during data collection was 3.0 × 3.0 μm^2. Rejection mirrors and a crystal Si(111) pair monochromator were used to prevent second-order harmonics. Four scans were collected and merged for each sample with energy calibrated against an Fe(0) foil (7112 eV). All spectra were energy calibrated in Athena,[27] and pre-edge subtracted, and post-edge normalized in SIXPack.[28] Shell-by-shell fits of k^3-weighted Fe EXAFS spectra were performed from 1 to 4 Å in $R+\Delta R$-space (k-range 2−12.5 Å) using SIXPack software, based on algorithms derived from IFEFFIT.[29] Phase and amplitude functions were calculated with FEFF6.[30] Fe-O and Fe-Fe scattering paths were derived from the structure of goethite[31] while Fe-P path was from strengite.[32] Following with previous work,[33] the passive electron reduction parameter, S_0^2, was set to 0.85 in all individual fits, and the mean squared atomic displacement parameter (σ^2) for Fe-Fe edge-sharing and corner-sharing path to 0.016 and 0.012, respectively.

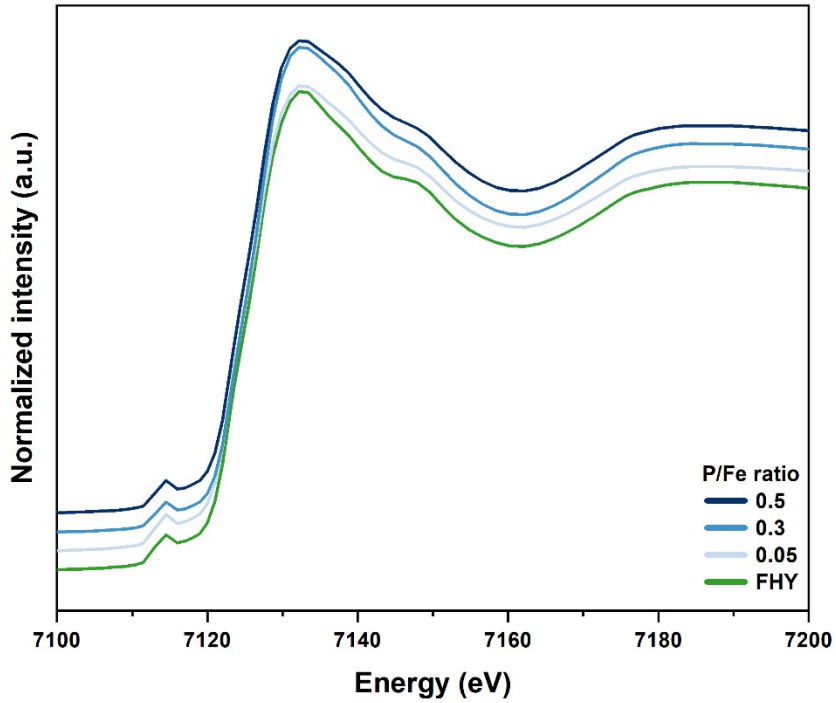

Figure S10. Fe K-edge XANES of GP-free and GP-FHY coprecipitates with nominal P/Fe molar ratios of 0.05, 0.3 and 0.5

Table S8. An example of fitting attempts for coprecipitate at P/Fe of 0.5

Atomic pair	CN	*R* (Å)	σ^2 (Å^2)	ΔE_0 (eV)	Red. X^2	R-factor
2 Fe-P paths						
Fe-O	4.4 (0.4)	1.98 (0.01)	0.010 (0.001)	-0.8 (0.8)	0.0314	0.0126
Fe-P1 (BB)	2.9 (1.0)	3.23 (0.01)	0.009 (0.003)			
Fe-P2 (BB)	0.7 (0.7)	3.60 (0.05)	σ^2 (Fe-P1)			
1 Fe-P and 1 Fe-Fe$_{edge}$						
Fe-O	4.4 (0.4)	1.98 (0.01)	0.010 (0.001)	-0.7 (0.8)	0.0295	0.0129
Fe-Fe$_{edge}$	1.0 (0.7)	3.04 (0.04)	*0.016*			
Fe-P1 (BB)	1.8 (0.6)	3.24 (0.01)	*0.007*			
2 Fe-P and 1 Fe-Fe$_{edge}$						
Fe-O	4.4 (0.4)	1.98 (0.01)	0.010 (0.001)	-0.8 (0.9)	0.0288	0.0105
Fe-Fe$_{edge}$	1.3 (0.8)	3.05 (0.03)	*0.016*			
Fe-P1 (BB)	1.5 (0.6)	3.25 (0.02)	*0.007*			
Fe-P2 (MM)	0.5 (0.3)	3.57 (0.05)	σ^2 (Fe-P1)			
1 Fe-P and 2 Fe-Fe						
Fe-O	4.4 (0.3)	1.98 (0.01)	0.010 (0.001)	-0.9 (0.8)	0.0247	0.0089
Fe-Fe$_{edge}$	1.6 (0.8)	3.06 (0.02)	*0.016*			
Fe-P1 (BB)	1.2 (0.6)	3.26 (0.03)	*0.007*			
Fe-Fe$_{corner}$	0.7 (0.4))	3.43 (0.04)	*0.012*			

The fitting result on the light blue background was adopted.

References

(1) Perez, J. P. H.; Freeman, H. M.; Schuessler, J. A.; Benning, L. G. The Interfacial Reactivity of Arsenic Species with Green Rust Sulfate (GRSO4). *Sci. Total Environ.* **2019**, *648*, 1161–1170. https://doi.org/10.1016/j.scitotenv.2018.08.163.

(2) Brunauer, S.; Emmett, P. H.; Teller, E. Adsorption of Gases in Multimolecular Layers. *J. Am. Chem. Soc.* **1938**, *60* (2), 309–319. https://doi.org/10.1021/ja01269a023.

(3) Rouquerol, J.; Rouquerol, F.; Llewellyn, P.; Maurin, G.; Sing, K. S. W. *Adsorption by Powders and Porous Solids: Principles, Methodology and Applications*; Academic Press, 2013.

(4) Barrett, E. P.; Joyner, L. G. Determination of Nitrogen Adsorption-Desorption Isotherms. *Anal. Chem.* **1951**, *23* (5), 791–792. https://doi.org/10.1021/ac60053a032.

(5) Mikutta, R.; Mikutta, C. Stabilization of Organic Matter at Micropores (<2 Nm) in Acid Forest Subsoils. *Soil Sci. Soc. Am. J.* **2006**.

(6) Santoro, V.; Martin, M.; Persson, P.; Lerda, C.; Said-Pullicino, D.; Magnacca, G.; Celi, L. Inorganic and Organic P Retention by Coprecipitation during Ferrous Iron Oxidation. *Geoderma* **2019**, *348*, 168–180. https://doi.org/10.1016/j.geoderma.2019.04.004.

(7) Pauw, B. R.; Smith, A. J.; Snow, T.; Terrill, N. J.; Thünemann, A. F. The Modular Small-Angle X-Ray Scattering Data Correction Sequence. *J. Appl. Crystallogr.* **2017**, *50* (6), 1800–1811. https://doi.org/10.1107/S1600576717015096.

(8) *dataMerge - A statistics-aware binning and merging backend*. figshare. https://doi.org/10.6084/m9.figshare.21591360.v1.

(9) Breßler, I.; Kohlbrecher, J.; Thünemann, A. F. SASfit: A Tool for Small-Angle Scattering Data Analysis Using a Library of Analytical Expressions. *J. Appl. Crystallogr.* **2015**, *48* (5), 1587–1598. https://doi.org/10.1107/S1600576715016544.

(10) Tejedor-Tejedor, M. I.; Anderson, M. A. The Protonation of Phosphate on the Surface of Goethite as Studied by CIR-FTIR and Electrophoretic Mobility. *Langmuir* **1990**, *6* (3), 602–611. https://doi.org/10.1021/la00093a015.

(11) Arai, Y.; Sparks, D. L. ATR–FTIR Spectroscopic Investigation on Phosphate Adsorption Mechanisms at the Ferrihydrite–Water Interface. *J. Colloid Interface Sci.* **2001**, *241* (2), 317–326. https://doi.org/10.1006/jcis.2001.7773.

(12) Cagnasso, M.; Boero, V.; Franchini, M. A.; Chorover, J. ATR-FTIR Studies of Phospholipid Vesicle Interactions with α-FeOOH and α-Fe2O3 Surfaces. *Colloids Surf. B Biointerfaces* **2010**, *76* (2), 456–467. https://doi.org/10.1016/j.colsurfb.2009.12.005.

(13) Li, H.; Wan, B.; Yan, Y.; Zhang, Y.; Cheng, W.; Feng, X. Adsorption of Glycerophosphate on Goethite (α-FeOOH): A Macroscopic and Infrared Spectroscopic Study. *J. Plant Nutr. Soil Sci.* **2018**, *181* (4), 557–565. https://doi.org/10.1002/jpln.201700517.

(14) Abdala, D. B.; Northrup, P. A.; Arai, Y.; Sparks, D. L. Surface Loading Effects on Orthophosphate Surface Complexation at the Goethite/Water Interface as Examined by Extended X-Ray Absorption Fine Structure (EXAFS) Spectroscopy. *J. Colloid Interface Sci.* **2015**, *437*, 297–303. https://doi.org/10.1016/j.jcis.2014.09.057.

(15) Phosphate adsorption onto hematite: An in situ ATR-FTIR investigation of the effects of pH and loading level on the mode of phosphate surface complexation. *J. Colloid Interface Sci.* **2007**, *308* (1), 53–70. https://doi.org/10.1016/j.jcis.2006.12.061.

(16) Omoike, A.; Chorover, J.; Kwon, K. D.; Kubicki, J. D. Adhesion of Bacterial Exopolymers to α-FeOOH: Inner-Sphere Complexation of Phosphodiester Groups. *Langmuir* **2004**, *20* (25), 11108–11114. https://doi.org/10.1021/la048597+.
(17) Olsson, R.; Giesler, R.; Loring, J. S.; Persson, P. Adsorption, Desorption, and Surface-Promoted Hydrolysis of Glucose-1-Phosphate in Aqueous Goethite (α-FeOOH) Suspensions. *Langmuir* **2010**, *26* (24), 18760–18770. https://doi.org/10.1021/la1026152.
(18) Persson, P.; Andersson, T.; Nelson, H.; Sjöberg, S.; Giesler, R.; Lövgren, L. Surface Complexes of Monomethyl Phosphate Stabilized by Hydrogen Bonding on Goethite (α-FeOOH) Nanoparticles. *J. Colloid Interface Sci.* **2012**, *386* (1), 350–358. https://doi.org/10.1016/j.jcis.2012.07.042.
(19) He, Q.; Reis, C. E. R.; Wang, F.; Hu, B. Phytate Extraction from Coproducts of the Dry-Grind Corn Ethanol Process. *RSC Adv.* **2017**, *7* (9), 5466–5472. https://doi.org/10.1039/C6RA27409A.
(20) Kwon, K. D.; Kubicki, J. D. Molecular Orbital Theory Study on Surface Complex Structures of Phosphates to Iron Hydroxides: Calculation of Vibrational Frequencies and Adsorption Energies. *Langmuir* **2004**, *20* (21), 9249–9254. https://doi.org/10.1021/la0487444.
(21) Yan, W.; Jing, C. Molecular Insights into Glyphosate Adsorption to Goethite Gained from ATR-FTIR, Two-Dimensional Correlation Spectroscopy, and DFT Study. *Environ. Sci. Technol.* **2018**, *52* (4), 1946–1953. https://doi.org/10.1021/acs.est.7b05643.
(22) Barja, B. C.; dos Santos Afonso, M. Aminomethylphosphonic Acid and Glyphosate Adsorption onto Goethite: A Comparative Study. *Environ. Sci. Technol.* **2005**, *39* (2), 585–592. https://doi.org/10.1021/es035055q.
(23) Cornell, R. M.; Schwertmann, U. *Iron Oxides: Structure, Properties, Reactions, Occurences and Uses*, Second.; Wiley-VCH Verlag GmbH & Co.: KGaA: Weinheim, FRG, 2000.
(24) Ristić, M.; De Grave, E.; Musić, S.; Popović, S.; Orehovec, Z. Transformation of Low Crystalline Ferrihydrite to α-Fe2O3 in the Solid State. *J. Mol. Struct.* **2007**, *834–836*, 454–460. https://doi.org/10.1016/j.molstruc.2006.10.016.
(25) Benning, L. G.; Phoenix, V. R.; Yee, N.; Tobin, M. J. Molecular Characterization of Cyanobacterial Silicification Using Synchrotron Infrared Micro-Spectroscopy. *Geochim. Cosmochim. Acta* **2004**, *68* (4), 729–741. https://doi.org/10.1016/S0016-7037(03)00489-7.
(26) Klementiev, K.; Chernikov, R. XAFSmass: A Program for Calculating the Optimal Mass of XAFS Samples. *J. Phys. Conf. Ser.* **2016**, *712*, 012008. https://doi.org/10.1088/1742-6596/712/1/012008.
(27) Ravel, B.; Newville, M. ATHENA, ARTEMIS, HEPHAESTUS: Data Analysis for X-Ray Absorption Spectroscopy Using IFEFFIT. *J. Synchrotron Radiat.* **2005**, *12* (4), 537–541. https://doi.org/10.1107/S0909049505012719.
(28) Webb, S. M. SIXpack: A Graphical User Interface for XAS Analysis Using IFEFFIT. *Phys. Scr.* **2005**, *2005* (T115), 1011. https://doi.org/10.1238/Physica.Topical.115a01011.
(29) Newville, M.; IUCr. *IFEFFIT : interactive XAFS analysis and FEFF fitting*. Journal of Synchrotron Radiation. https://doi.org/10.1107/S0909049500016964.
(30) Rehr, J. J.; Albers, R. C.; Zabinsky, S. I. High-Order Multiple-Scattering Calculations of x-Ray-Absorption Fine Structure. *Phys. Rev. Lett.* **1992**, *69* (23), 3397–3400. https://doi.org/10.1103/PhysRevLett.69.3397.

(31) Kaur, N.; Singh, B.; Kennedy, B. J.; Gräfe, M. The Preparation and Characterization of Vanadium-Substituted Goethite: The Importance of Temperature. *Geochim. Cosmochim. Acta* **2009**, *73* (3), 582–593. https://doi.org/10.1016/j.gca.2008.10.025.
(32) Taxer, K.; Bartl, H. On the dimorphy between the variscite and clinovariscite group: refined finestructural relationship of strengite and clinostrengite, Fe(PO4) . 2H2O. *Cryst. Res. Technol.* **2004**, *39* (12), 1080–1088. https://doi.org/10.1002/crat.200410293.
(33) Voegelin, A.; Kaegi, R.; Frommer, J.; Vantelon, D.; Hug, S. J. Effect of Phosphate, Silicate, and Ca on Fe(III)-Precipitates Formed in Aerated Fe(II)- and As(III)-Containing Water Studied by X-Ray Absorption Spectroscopy. *Geochim. Cosmochim. Acta* **2010**, *74* (1), 164–186. https://doi.org/10.1016/j.gca.2009.09.020.